# Genome-Wide Chromatin Structure Changes During Adipogenesis and Myogenesis

Mengnan He[1,2*], Yan Li[1,2*], Qianzi Tang[1,2*], Diyan Li[1,2], Long Jin[1,2], Shilin Tian[3], Tiandong Che[1,2], Shen He[1,2], Lamei Deng[3], Guangliang Gao[1,2,4], Yiren Gu[5], Zhi Jiang[3], Xuewei Li[1,2]✉ & Mingzhou Li[1,2]✉

1. Institute of Animal Genetics and Breeding, College of Animal Science and Technology, Sichuan Agricultural University, Chengdu 611130, China;
2. Farm Animal Genetic Resources Exploration and Innovation Key Laboratory of Sichuan Province, Sichuan Agricultural University, Chengdu 611130, China;
3. Novogene Bioinformatics Institute, Beijing 100089, China;
4. Chongqing Academy of Animal Sciences, Chongqing 402460, China;
5. Animal Breeding and Genetics Key Laboratory of Sichuan Province, Pig Science Institute, Sichuan Animal Science Academy, Chengdu 610066, China.

*These authors contributed equally to this work.

✉Corresponding authors:

Mingzhou Li, E-mail: mingzhou.li@sicau.edu.cn;

Xuewei Li, E-mail: xuewei.li@sicau.edu.cn.

## Supplementary Tables

**Table S1. Mapping statistics and data quality of Hi-C sequencing (25328f2_suppl1.xlsx)**

**Table S2. Data source information**

**Table S3. RNA-seq data description**

**Table S4. Functional enrichment analysis of upregulated genes in compartment B to A during differentiation (25328f2_suppl2.xlsx)**

**Table S5. Upregulated DEGs in highly promoter-associated interactions during adipogenesis and myogenesis (25328f2_suppl3.xlsx)**

**Table S2. Data source information**

| Data description | Source | IDENTIFIER |
|---|---|---|
| H3K4me3 ChIP-seq 3T3-L1 pre-adipocytes | Matsumura Y, et al. | GSM 1893623 |
| H3K4me3 ChIP-seq C2C12 myoblasts | Jiang L, et al. | GSM 822510 |
| ATAC-seq C2C12 myoblasts | Dell'Orso S, et al. | GSM 1972411 |
| ATAC-seq C2C12-D myotubes | Dell'Orso S, et al. | GSM 1972413 |
| CTCF ChIP-seq 3T3-L1 pre-adipocytes | Siersbæk R, et al. | GSM 2515926 |
| CTCF ChIP-seq C2C12 myoblasts | Beer MA, et al. | GSM 915188 |
| Predicted mouse enhancer | FANTOM5 Data | http://fantom.gsc.riken.jp/5/datafiles/latest/extra/Enhancers/ |
| Cebpb ChIP-seq 3T3-L1 pre-adipocytes | Siersbæk R, et al. | GSM686970 |
| Cebpa ChIP-seq 3T3-L1-D adipocytes | Step SE, et al. | GSM1368011 |
| Cebpb ChIP-seq 3T3-L1-D adipocytes | Siersbæk R, et al. | GSM686973 |
| Pparg ChIP-seq 3T3-L1-D adipocytes | Mikkelsen TS, et al. | GSM535769 |
| Myod ChIP-seq C2C12 myoblasts | Beer MA, et al. | GSM915186 |
| Myog ChIP-seq C2C12 myoblasts | Beer MA, et al. | GSM915166 |
| Myod ChIP-seq C2C12-D myotubes | Beer MA, et al. | GSM915165 |
| Myog ChIP-seq C2C12-D myotubes | Beer MA, et al. | GSM915164 |
| MEF2A ChIP-seq C2C12-D myotubes | Wales S, et al. | GSM1499534 |
| MEF2D ChIP-seq C2C12-D myotubes | Sebastian S, et al. | GSM1058956 |

**Table S3. RNA-seq data description**

| Sample name | Raw data (Gb) | Error ratio (%) | Q20 (%) | Q30 (%) | GC (%) | High quality data (bp) | Mapped data (Gb) | Mapping ratio (%) | Expressed protein coding genes (FPKM > 0.5) | Genes with FPKM > 0.5 (at least in one sample) |
|---|---|---|---|---|---|---|---|---|---|---|
| 3T3-L1 | 11.93 | 0.04 | 93.49 | 88.11 | 50.45 | 11.79 | 11.07 | 93.9 | 11,204 | 12,753 |
| 3T3-L1-D | 11.33 | 0.04 | 93.82 | 88.57 | 49.93 | 11.18 | 10.47 | 93.6 | 11,347 | 12,753 |
| C2C12 | 10.80 | 0.04 | 93.66 | 88.37 | 50.29 | 10.61 | 9.71 | 91.5 | 11,096 | 12,753 |
| C2C12-D | 12.53 | 0.04 | 93.52 | 88.15 | 50.66 | 12.39 | 11.61 | 93.8 | 11,458 | 12,753 |

## Supplementary Figures

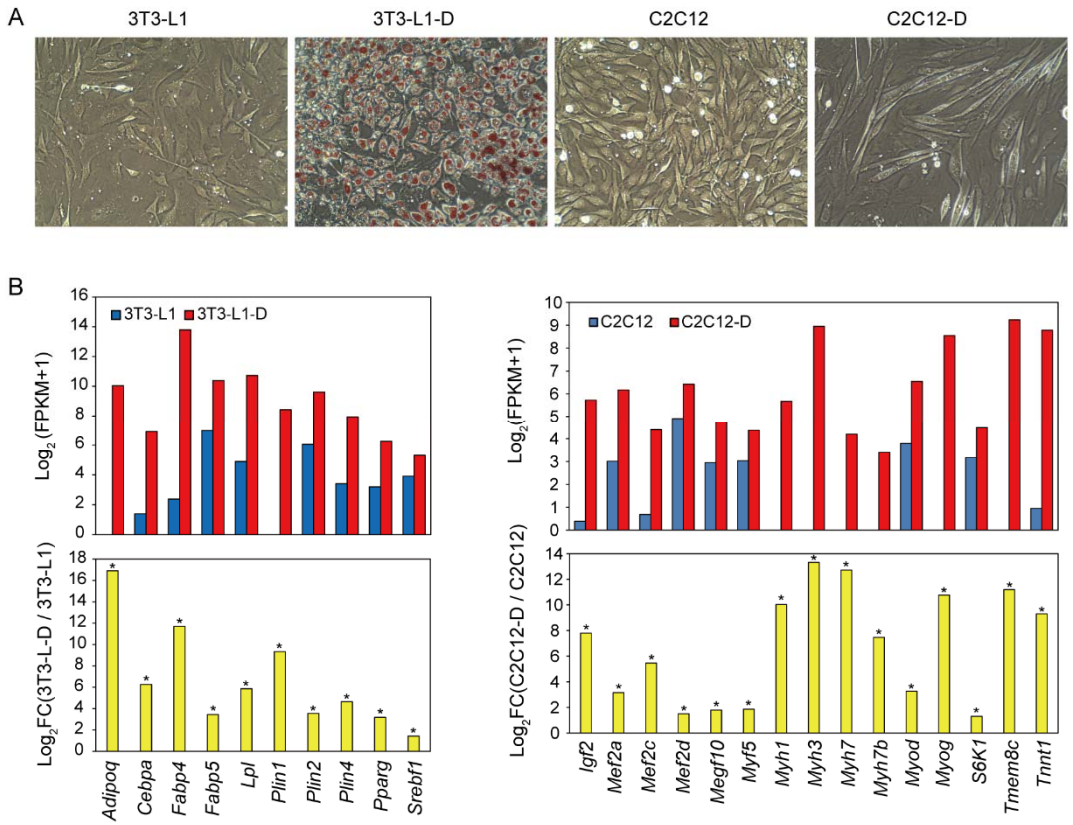


**Figure S1. Adipogenic and myogenic differentiation cell models.**

(A) Images of 3T3-L1 pre-adipocytes, 3T3-L1-D adipocytes, C2C12 myoblasts, and C2C12-D myotubes. Proliferating 3T3-L1 have fibroblast-like morphology and C2C12 are spindle-shaped mononucleated myoblasts. Oil Red O-stained 3T3-L1-D (day 10) showed numerous lipid droplets. Most myogenic differentiated C2C12-D (day 8) were multinucleated myotubes.

(B) Adipogenic and myogenic marker genes were significantly upregulated after differentiation. These marker genes are well known and reported by publications. Differential expression analysis was performed by DEG-seq. Fold change (FC) is ratio of $\log_2$(FPKM+1), the Asterisk indicates $P < 0.001$ and FDR < 0.05.

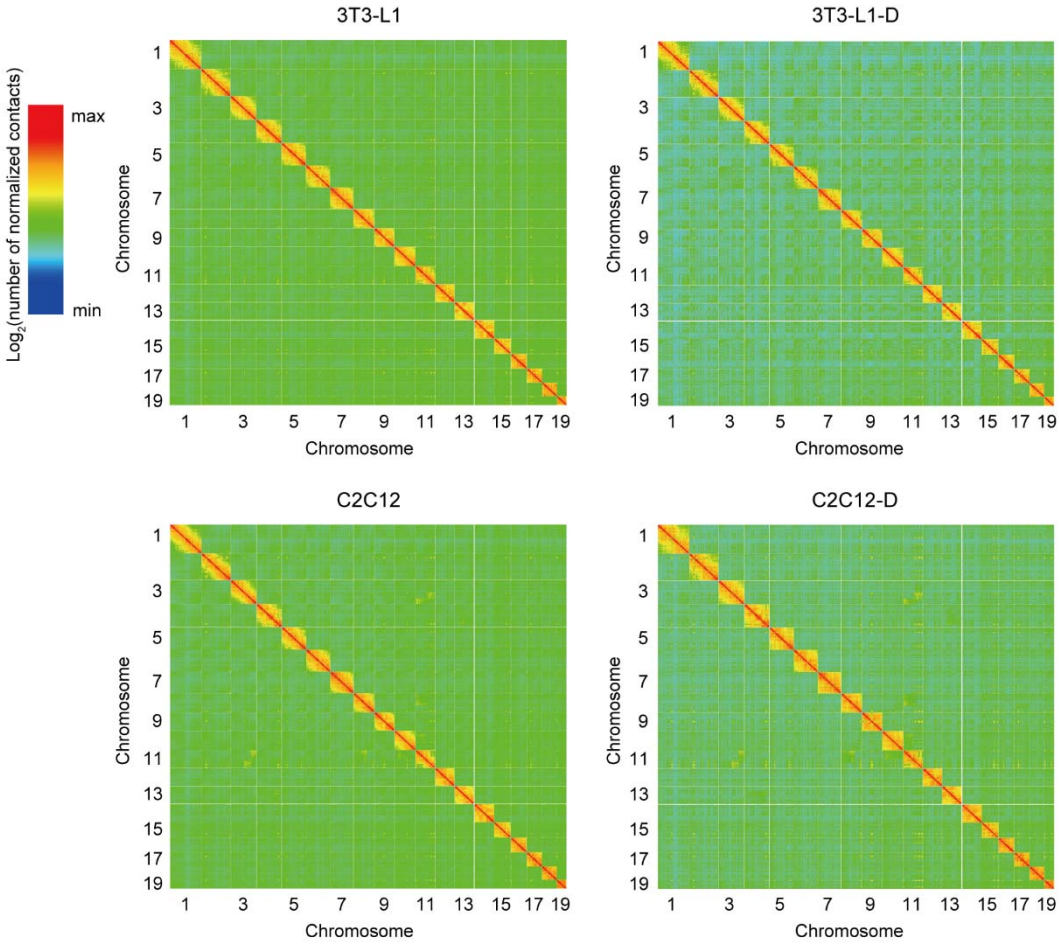


**Figure S2. Genome-wide chromatin interaction maps of four cell types.**

Heat maps represent the genome-wide chromatin interaction map at 1-Mb resolution. Color intensity indicates the $\log_2$ of normalized number of Hi-C contacts from each pair of interacting fragments. The unalignable region is indicated in gray.

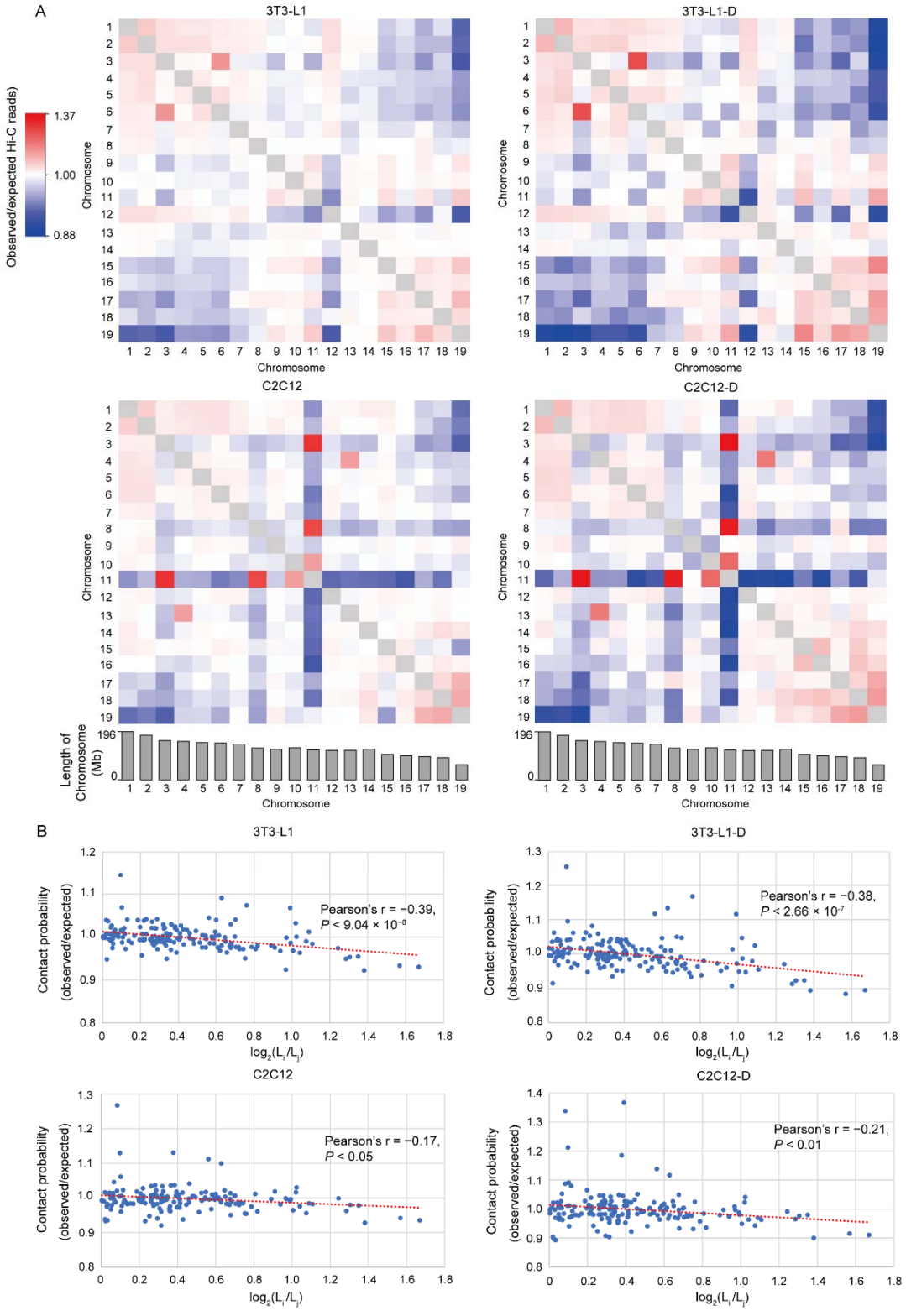


**Figure S3. *Trans* interactions exhibited two large territories with similar chromosome lengths.**

(A) Observed/expected number of contacts between any pairs of 19 euchromosomes. Red indicates enrichment, blue indicates depletion. Gray histogram indicates chromosome length (Mb) of each chromosome.
(B) The observed/expected number of interactions between any pair of 19 euchromosomes plotted against the difference in the lengths of those chromosomes. Length difference is indicated by $\log_2 L_i/L_j$, $L_i$ or $L_j$ is the length of chromosome, $L_i > L_j$. The dotted lined represents the linear trend for obtained values.

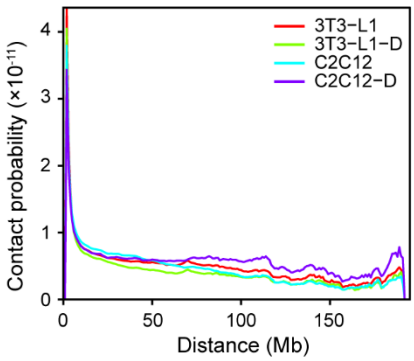


**Figure S4. The interaction frequency decreased with increasing genomic distance.** The contact probability at a given genomic distance was the mean of all *cis* interactions at that genomic distance. The total range of genomic distance is the length of the largest chromosome.

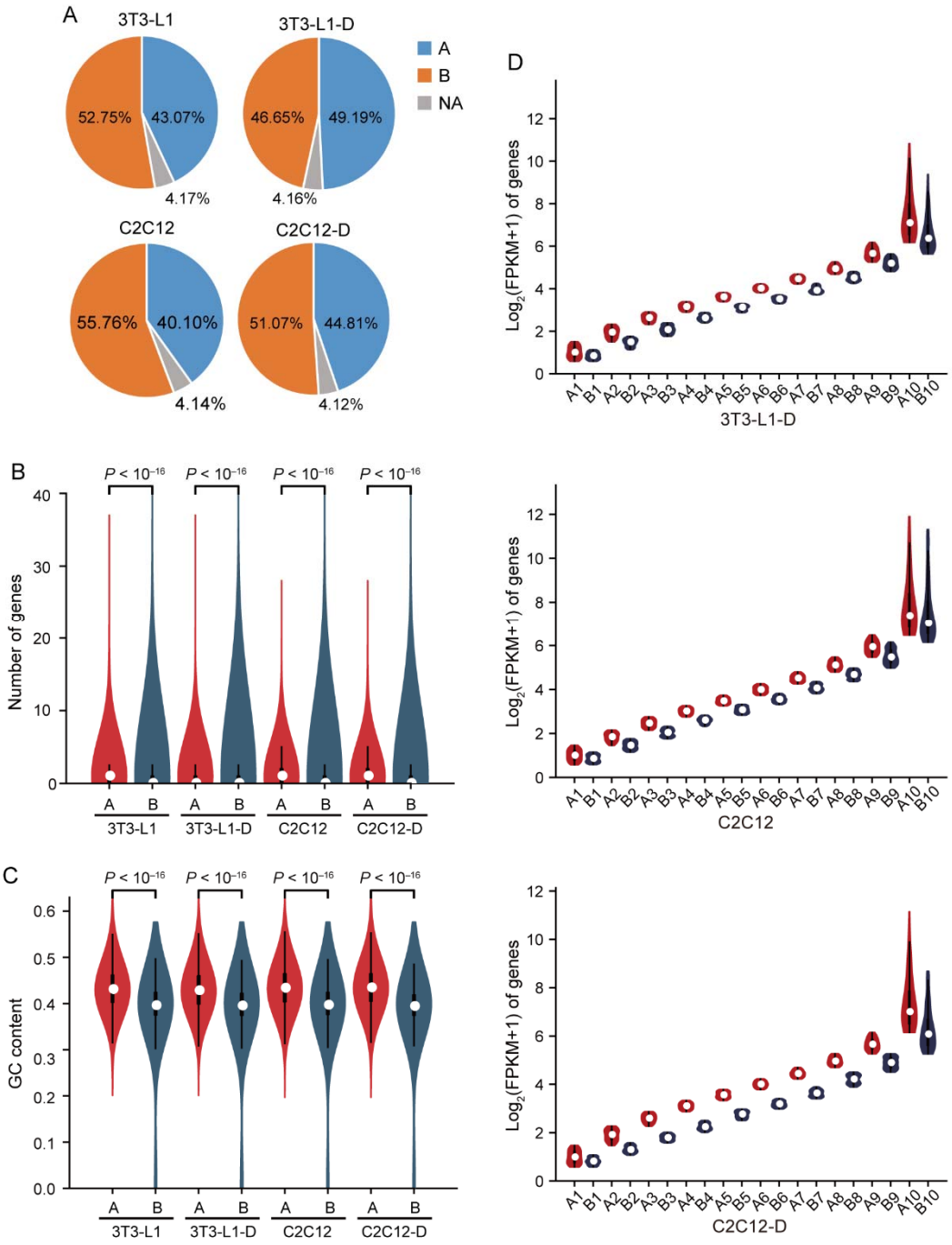


**Figure S5. Consensus and intrinsic compartment A/B characteristics in four cell types.**

(A) Proportion of the genome in the compartment A (blue) or B (orange) in each of the four cell types. Shown in gray are regions with a PC1 of zero, often corresponding to centromeric and telomeric regions of the chromosomes.

(B) Number of genes in compartment A is significantly higher than in B (40 kb), 0.93 vs. 0.58, 0.91 vs. 0.56, 0.96 vs. 0.58, and 0.96 vs. 0.54 in each cell type (Wilcoxon's test, $P < 10^{-16}$).

(C) GC content in compartment A is significantly higher than in B (40kb), 0.43 vs. 0.38, 0.43 vs. 0.38, 0.44 vs. 0.39, and 0.44 vs. 0.38 in each cell type (Wilcoxon's test, $P < 10^{-16}$).

(D) Gene expression levels in compartment A are significantly higher than in B at each cluster of 3T3-L1-D, C2C12, and C2C12-D, the same as in Figure 4B (Wilcoxon's test, $P < 10^{-16}$ for each pair of compartment A vs. B).

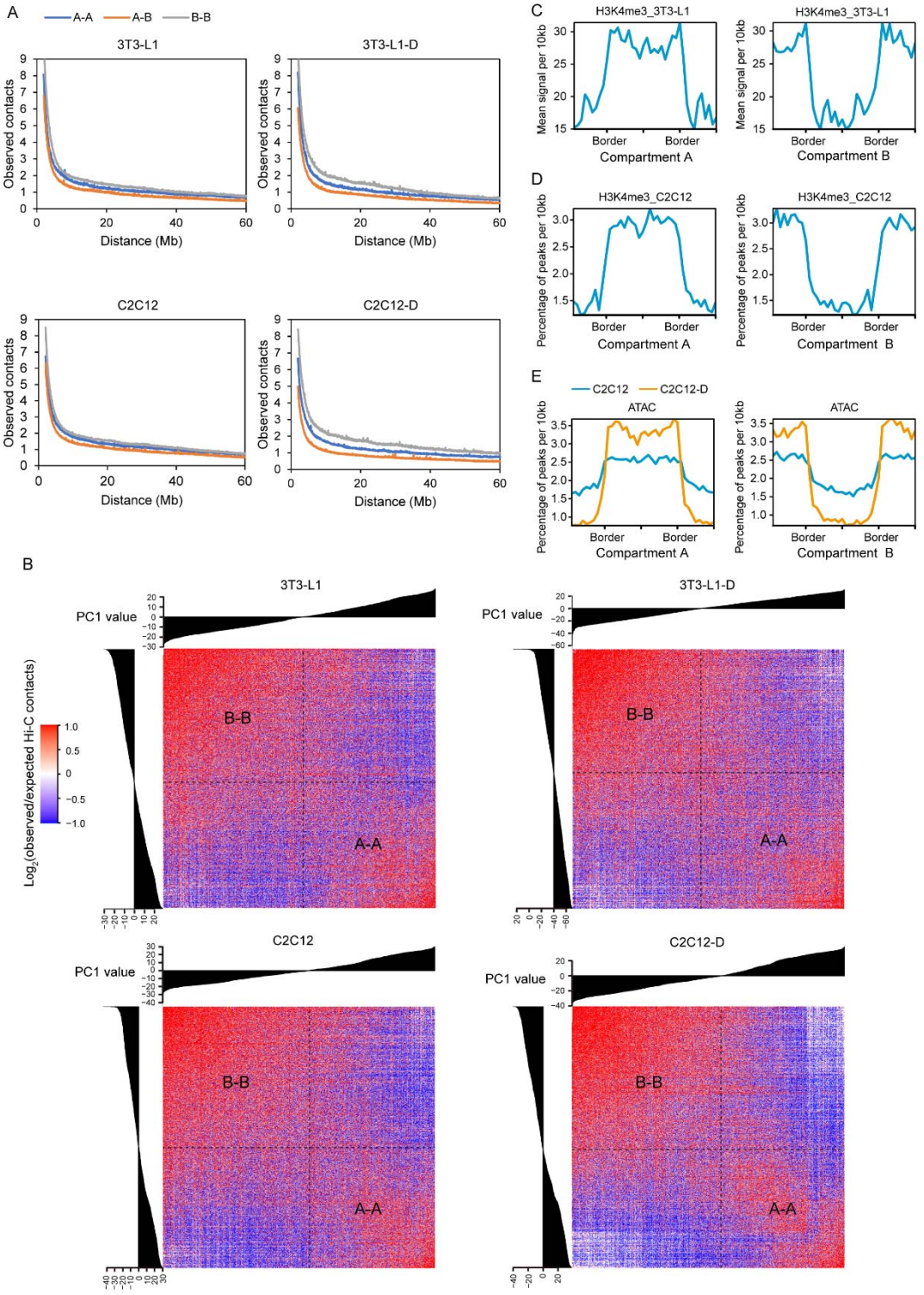


72

73 **Figure S6. More active chromatin state of compartment A than of compartment B.**

74 (A) Compartment A is less compact than compartment B. Contact enrichment as a

75 function of distance for interactions between bins in noncontiguous blocks belonging

to the same compartment A (A-A) or B (B-B), and interactions between different compartments A and B (A-B).

(B) Mean contact enrichment between pairs of 40-kb bins arranged by their PC1 value.

(C) ChIP-seq signal enrichment of H3K4me3 in compartments A and B of 3T3-L1.

(D) ChIP-seq peak enrichment of H3K4me3 in compartments A and B of C2C12.

(E) Chromatin accessibility of compartments A and B indicated by ATAC-seq peak enrichment in C2C12 and C2C12-D.

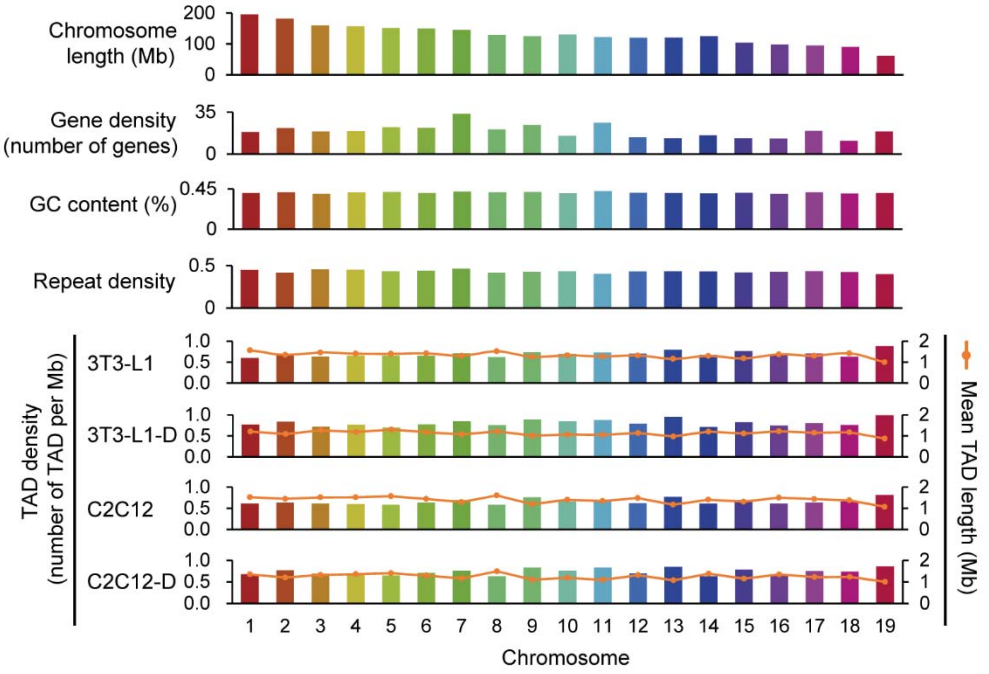


86

87 **Figure S7. TAD description in each chromosome.** Chromosome length, gene density,

88 GC content, repeat density, and TAD density of each chromosome are shown.

89

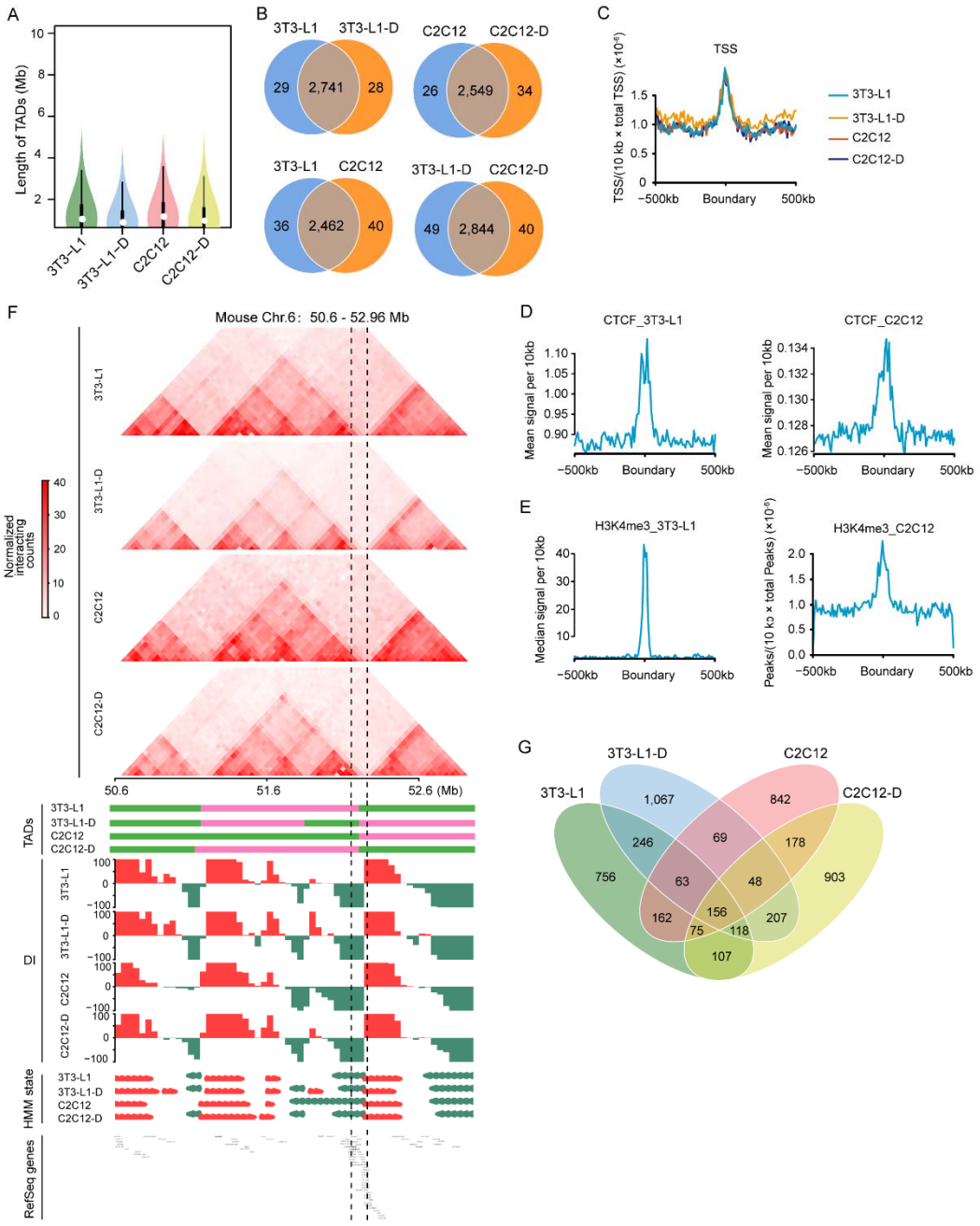


**Figure S8. Conserved TAD boundaries during differentiation and between cell types.**

(A) Violin plot showing TAD size distribution in four cell types. White dot in the box indicates the median TAD size. Detailed statistics of TAD number and size are described in Table 1.

(B) Overlap of TAD boundaries between cell types ($P < 10^{-16}$ compared with random, Fisher's exact test).

(C–E) TAD boundary characteristics. TSS (C), architectural protein CTCF (D), and active histone mark H3K4me3 (E) are enriched in TAD boundaries.

(F) Species-conserved *Hoxa* locus is separated by two TADs in four cell types. The region between the black dashed lines represents the *Hoxa* gene cluster (Chr.6: 52,155,590–52,260,880). Green and pink lines represent different TADs.

(G) Overlap of completely stable TADs in four cell types.

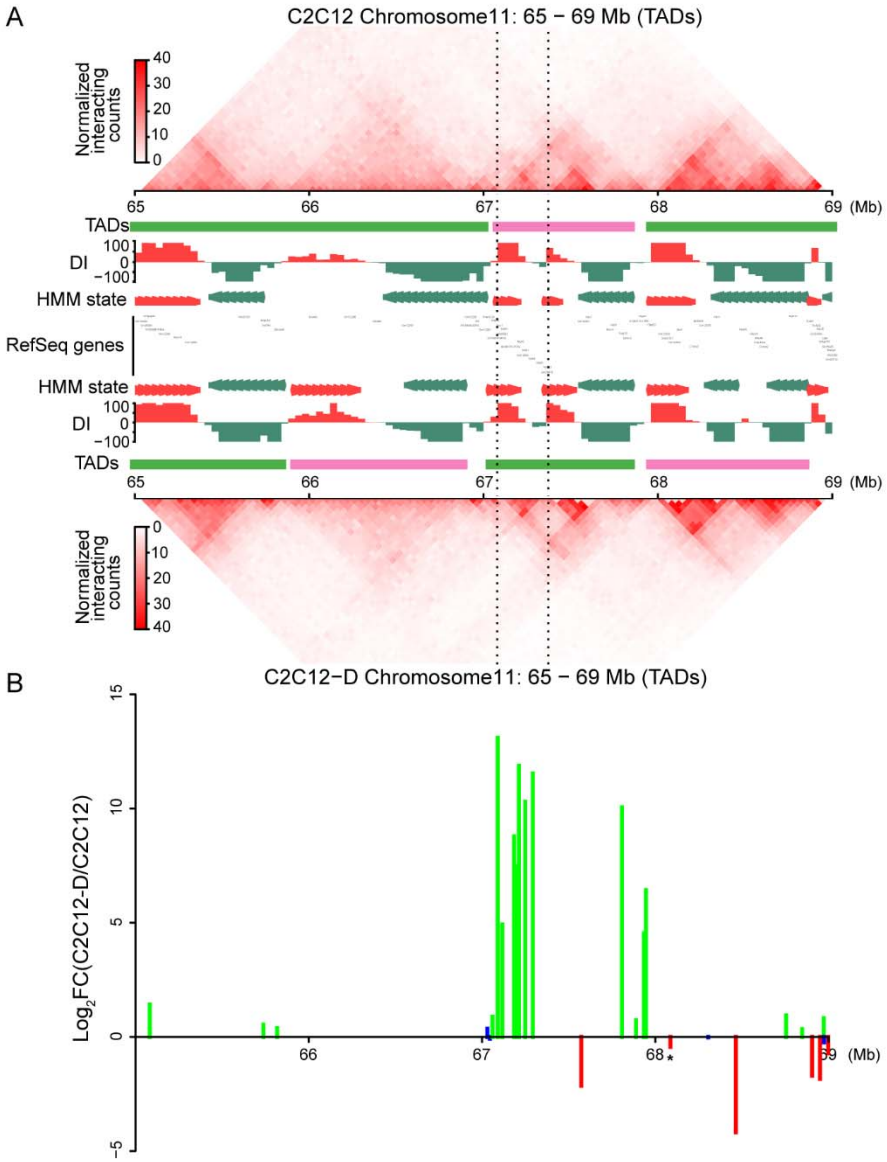


**Figure S9. Myogenic differentiation generated myotube-specific chromatin interactions and correlated with gene activity.**

(A) Genome browser shots showing domain structure of a 5-Mb region over *Myhc* gene clusters in C2C12 (top panel) and C2C12-D (bottom panel). The region between the black dashed lines represents the *Myh3/2/1/4/8/13* gene cluster. Green and pink lines represent different TADs. The *Myhc* gene cluster-located TAD was stable but showed an intensification of local interaction frequency near the *Myhc* gene cluster.

(B) The *Myhc* gene cluster was activated with significantly upregulated gene expression. The green lines indicate upregulated DEGs and red lines indicate downregulated ones, blue lines refer to non-DEGs.

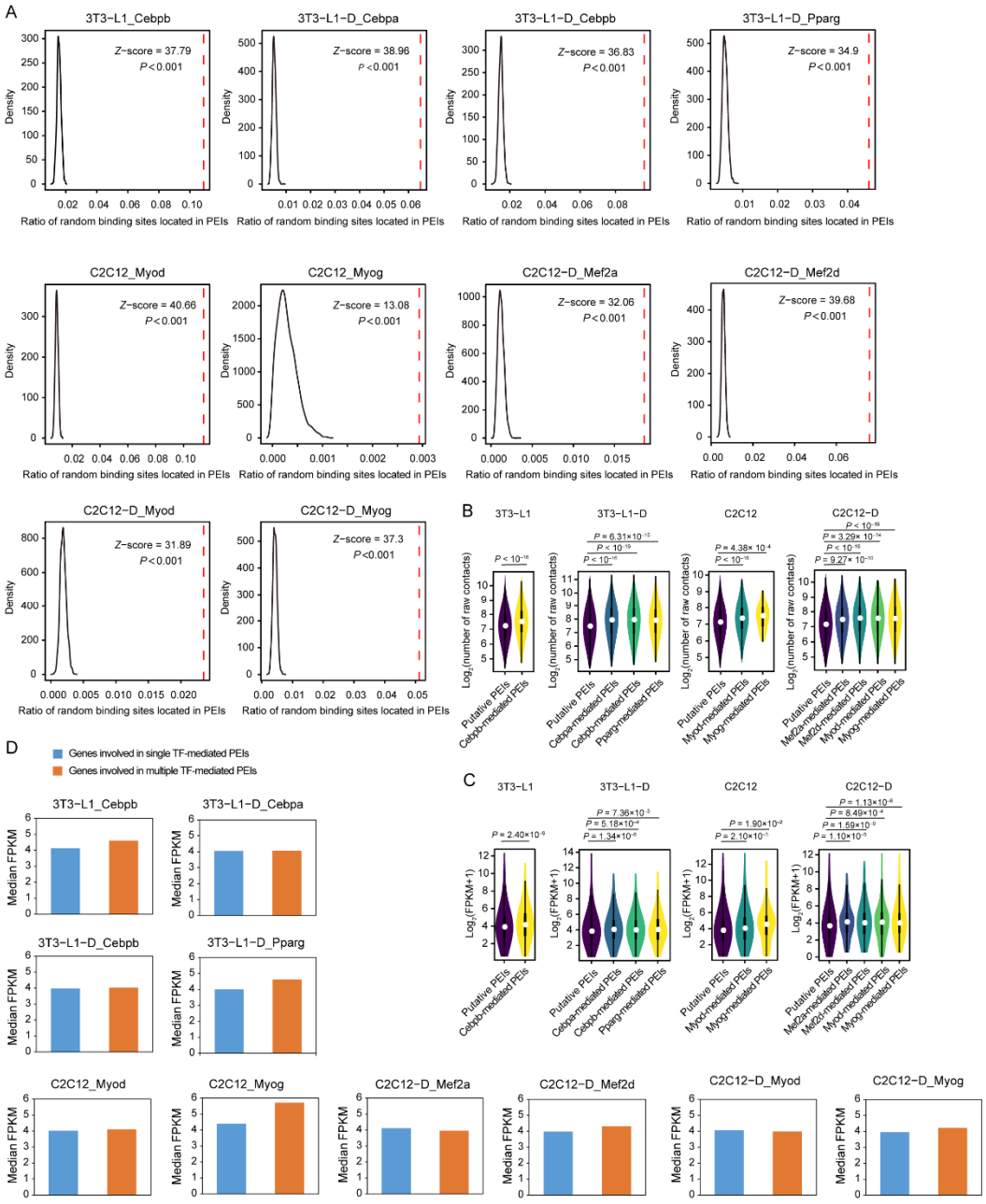


**Figure S10. Typical adipogenic and myogenic TFs mediated gene expression via the formation of promoter–enhancer interactions.**

(A) Compared with random binding sites, transcription factor (TF) binding sites were enriched in enhancer regions of putative promoter–enhancer interactions (PEIs). The black curve indicates the distribution of the ratio of random binding sites located in enhancer regions of putative PEIs. The red dotted line indicates the ratio of TF binding

sites located in enhancer regions of putative PEIs. *P* values were obtained by the *z*-score transformation of these ratios ($P < 0.001$).

(B) TF-mediated PEIs showed significantly higher interaction strength than putative PEIs, which may include many silent enhancer regions in PEIs (Wilcoxon's test, $P < 0.001$).

(C) Genes involved in TF-mediated PEIs showed significantly higher expression level than those in putative PEIs (Wilcoxon's test, $P < 0.02$).

(D) Genes involved in multiple TF-mediated PEIs showed slightly higher expression level than those involved in single TF-mediated PEI.